Inorg. Chem. **2006**, *45*, 779–786

Luminescence Detection of Transition and Heavy Metals by Inversion of Excited States: Synthesis, Spectroscopy, and X-ray Crystallography of Ca, Mn, Pb, and Zn Complexes of 1,8-Anthraquinone-18-Crown-5

Mariappan Kadarkaraisamy and Andrew G. Sykes*

Contribution from the Department of Chemistry, University of South Dakota, Vermillion, South Dakota 57069

Received September 28, 2005

A lumophore composed of anthraquinone attached to a macrocyclic polyether ring containing an intraannular carbonyl is capable of selectively detecting Pb^{2+} ion in solution using an alternative photophysical detection mechanism. Of the various methods available for detection of ions in solution, a mechanism involving inversion of excited states has not been previously employed for the detection of transition and heavy metals. In this mechanism, nonradiative n–π* transitions are replaced by radiative π–π* transitions upon complexation by a suitable guest cation. Optimum fluorescence enhancement is achieved using cations of high charge, large cations that form long bonds within the host, and cations which do not coordinate solvent or the counteranion, all of which are necessary for inversion of excited states to occur. Photophysical properties and binding constants of this new class of luminescence sensors are provided, as well as the X-ray crystallographic results for Pb^{2+}, Mn^{2+}, and Zn^{2+} complexes of 1,8-oxybis-(ethylene-oxyethyleneoxy)anthracene-9,10-dione (**1**), referred to as 1,8-anthraquinone-18-crown-5. ([**1**·Pb]$(ClO_4)_2$ (**2**) (monoclinic, *P*21/*n*, $a = 8.0303(6)$ Å, $b = 25.976(2)$ Å, $c = 12.1616(9)$ Å, $\beta = 94.956(1)°$, $Z = 4$, 4980 reflections [$I \geq 2\sigma(I)$], R1 = 0.0266, wR2, 0.0500, 173(2) K). [**1**·Mn$(H_2O)(NCCH_3)$]$(ClO_4)_2$ (**5**) (monoclinic, *P*21/*c*, $a = 10.132(2)$ Å, $b = 11.8030(4)$ Å, $c = 23.999(7)$ Å, $\beta = 95.75(2)°$, $Z = 4$, 3000 reflections [$I \geq 2\sigma(I)$], R1 = 0.0488, wR2, 0.0938, 203(2) K). [**1**·Zn$(H_2O)(NCCH_3)$]$(ClO_4)_2$ (**6**) (monoclinic, *P*21/*c*, $a = 10.177(10)$ Å, $b = 11.977-(6)$ Å, $c = 24.166(4)$ Å, $\beta = 95.83(4)°$, $Z = 4$, 3061 reflections [$I \geq 2\sigma(I)$], R1 = 0.0673, wR2, 0.1729, 295(2) K).)

Introduction

Photoinduced electron transfer (PET) is the current, dominant photophysical mechanism for sensing metal ions in solution. In PET, receptors typically quench an adjacent lumophore via internal electron transfer, leaving the sensor in the 'off' state. Upon complexation of the receptor with a suitable guest, electron transfer is interrupted and luminescence is switched 'on'. There are roughly 6000 references to *Photoinduced Electron Transfer* in the chemical literature presently, and several review papers have been published.[1]

In this paper, we employ an alternative photophysical mechanism for the detection of metal ions in solution, one we feel holds significant promise in the field of luminescence sensors. With this mechanism, molecules with a low-lying n$-\pi$* transition generally do not luminesce; however, coordination of the lumophore's associated nonbonded electrons with an electropositive center raises the energy of the n$-\pi$* transition above that of the corresponding $\pi-\pi$* transition, and luminescence is switched 'on'. This photodynamic mechanism has previously been employed using molecules that have a unique response in various solvents. Pyrene-3-carboxaldehyde, dissolved in a nonpolar solvent, has a low-lying n$-\pi$* transition that renders this molecule nonluminescent. However, in methanol, hydrogen-bonding interactions with the carbonyl oxygen lone pairs increase the energy of the n$-\pi$* transition and is replaced by an emissive $\pi-\pi$* transition.[2] Consequently, fluorescence efficiency increases 100-fold between these two solvents. In a series of recent papers, we have pioneered the sensor based on **1**

* To whom correspondence should be addressed. E-mail: asykes@usd.edu.

(1) (a) de Silva, A. P.; McClean, G. D.; Moody, T. S.; Weir, S. M. *Handb. Photochem. Photobiol.* **2003**, *3*, 217. (b) de Silva, A. P.; Fox, D. B.; Huxley, A.; Moody, T. S. *Coord. Chem. Rev.* **2000**, *205*, 41. (c) de Silva, A. P.; Gunaratne, H. Q. N.; Gunnlaugsson, T.; Huxley, A. J. M.; McCoy, C. P.; Rademacher, J. T.; Rice, T. E. *Chem. Rev.* **1997**, *97*, 1515 and references within. (d) *Fluorescent Chemosensors for Ion and Molecular Recognition*; Czarnik, A. W., Ed.; American Chemical Society: Washington, DC, 1992. (e) Rurack, K. *Spectrochim. Acta* **2001**, *A57*, 2161.

10.1021/ic051672z CCC: $33.50
Published on Web 12/27/2005

(below), which is responsive to common oxoacids.[3] Hydronium ion is encapsulated within the crown ether and forms strong hydrogen bonds to the intraannular carbonyl oxygen, resulting in a dramatic increase in luminescence efficiency. This molecule has previously found utility as a redox-switchable crown ether that has a high affinity and selectivity for alkali metals in its electrochemically reduced state.[4]

Inversion of n−π* and π−π* states has also been previously employed in azoaromatic-based sensors, such as acridine, 1,10-phenanthroline derivatives, quinolines, and 2,2′-bipyridyl-containing macrocycles,[5] where the imine nitrogens chelate alkali metal ions; however, luminescence is generally limited to the UV region of the electromagnetic spectrum. Theoretical aspects of nonradiative and radiative decay from n−π* and π−π* transitions have also been addressed.[6] Recent examples include the detection of alkaline earth metals by a xanthone macrocycle that contains an intraannular carbonyl oxygen,[7a] the detection of Ca^{2+} and alkali metals by a tetranaphthylcalixarene,[7b] and the detection of Hg^{2+} by an 8-hydroxybenzoate.[7c] A novel fluorogenic probe that senses reaction chemistry by inversion of n−π* and π−π* states has also been described.[7d] Luminescence enhancement of the xanthone is hypothesized on the basis of a conformational change of the macrocycle, and luminescence occurs from a long-lived triplet state. None of these studies include crystallographic analyses of the complexes, however. This inversion mechanism may also play a roll in simple metal chelate complexes of α-hydroxy quinone compounds, such as those formed with alizarin and tetracycline, where luminescence has been attributed to charge transfer.[8] Here we report initial structure−property relationships of sensors that detect metal ions in solution and the solid state, including detection of lead with high selectivity. Several articles describing the fluorescence detection of lead ion using PET have previously been reported.[9]

Experimental Section

Reagents. 1,8-Oxybis(ethyleneoxyethyleneoxy)anthracene-9,10-dione (**1**) was synthesized using the reported procedure.[4a] Lead(II) perchlorate trihydrate (Aldrich), lead(II) nitrate (Fisher Scientific), calcium perchlorate tetrahydrate (Aldrich), manganese(II) perchlorate hexahydrate (Alfa Aesar), and zinc(II) perchlorate hexahydrate (Aldrich) were used as purchased. Elemental analyses were conducted by MHW Laboratories of Phoenix, AZ. Electrospray injection-mass spectrometry was conducted using a Micromass mass spectrometer (Manchester, UK). Melting points of all perchlorate salts exceed 300 °C. Fresh anhydrous acetonitrile (Fisher/Acros) was used in all spectroscopic studies, and perchlorate salts used in selectivity studies (Figure 5) were dried at 100 °C under vacuum over P_2O_5 to minimize effects of water of hydration; however, little difference was observed between the use of dried and undried perchlorate salts. Shock testing and melting point limit does not indicate an explosive nature of these perchlorate salts.

Preparation of Compounds. [Pb·1](ClO$_4$)$_2$ (2). 1 (0.3 g, 0.75 mmol) was dissolved in 20 mL of acetonitrile. Lead(II) perchlorate trihydrate (0.31 g, 0.75 mmol) was dissolved in 15 mL of acetonitrile and added dropwise to the above solution and stirred for 2 h. A pale yellow colored precipitate was obtained, filtered off, washed several times with diethyl ether, and air-dried. All the precipitate was dissolved in 20 mL of an acetonitrile−methanol (8:2) mixture, and layered with diethyl ether. Fine needle-shaped crystals were obtained. Yield ≈ 0.32 g, 50%. ESI MS: Calcd for $[Pb\cdot\mathbf{1}\cdot ClO_4]^+$ 705.07; found 705.01 (M^+, 100%). ^{1}H NMR (DMSO-d_6, 25 °C): δ 3.56 (m (broad), 4 H, CH_2−O); 3.67 (t, 4 H, CH_2−O, J = 2.8); 3.80 (m, 4 H, CH_2−O); 4.18 (m, 4 H, CH_2−O) 7.48 (m, 2H, Ar−H); 7.70 (m, 4 H, Ar−H). ^{13}C NMR (DMSO-d_6, 25 °C): δ 68.3, 69.1, 69.4, 70.2, 109.5, 118.2, 119.4, 124.1, 134.2, 157.7, 182.2, 183.6. Anal. Calcd for a [Pb·**1**][ClO$_4$]$_2$ sample dried at 100 °C in a vacuum ($C_{22}H_{22}$ $Cl_2O_{15}Pb$): C, 32.84; H, 2.73%. Found: C, 32.71; H, 2.64%. There was only a small amount of nitrogen present in an air-dried sample.

[Pb·1](NO$_3$)$_2$ (3). 1 (0.25 g, 0.63 mmol) was dissolved in acetonitrile and mixed with lead(II) nitrate (0.21 g, 0.63 mmol) made in 5 mL of water. The solution was stirred for 2 h. A pale yellow colored precipitate was obtained, filtered off, and washed several times with diethyl ether. All the precipitate was dissolved in 20 mL of DMF, and layered with diethyl ether. A pale yellow-colored fibrous solid was obtained. Yield ≈ 0.23 g, 51%. mp = 283−85 °C. ESI MS: Calcd for $[Pb\cdot\mathbf{1}\cdot NO_3]^+$ 667.42; found 667.11 (M^+, 100%). ^{1}H NMR (DMSO-d_6, 25 °C): δ 3.53 (*t*, 4 H, CH_2−O, J = 2.8); 3.62 (*t*, 4 H, CH_2−O, J = 2.8); 3.70 (*t* (broad), 4 H, CH_2−O); 4.14 (*t*, 4 H, CH_2−O, J = 2.4); 7.42 (*m*, 2H, Ar−H); 7.64 (*m*, 4 H, Ar−H). ^{13}C NMR (DMSO-d_6, 25 °C): δ 68.7, 69.4, 69.8, 70.6, 109.5, 118.6, 119.7, 124.3, 134.5, 134.8; 158.0, 163.3; 182.0, 184.1. Anal. Calcd for $C_{22}H_{22}O_{13}PbN_2$: C, 36.21; H, 3.02; N, 3.83%. Found: C, 36.36; H, 3.12; N, 4.02%.

(2) (a) Kalyanasundaram, K.; Thomas, J. K. *J. Phys. Chem.* **1977**, *81*, 2176. (b) Lianos, P.; Lux, B.; Gerald, D. J. *Chim. Phys.* **1988**, *77*, 907.

(3) (a) Kadarkaraisamy, M.; Dufek, E.; Lone Elk, D.; Sykes, A. G. *Tetrahedron* **2005**, *61*, 479. (b) Kampmann, B.; Lian, Y.; Klinkel, K.; Vecchi, P. A.; Quiring, H. L.; Soh, C. C.; Sykes, A. G. *J. Org. Chem.* **2002**, *67*(11), 3878−3883. (c) Young, V., Jr.; Sykes, A. G. *Inorg. Chem.* **1998**, *37*, 376. (d) Young, V. G., Jr.; Quiring, H. L.; Sykes, A. G. *J. Am. Chem. Soc.* **1997**, *119*, 12477.

(4) (a) Delgado, M.; Gustowski, D. A.; Yoo, H. K.; Gatto, V. J.; Gokel G. W.; Echegoyen, L. *J. Am. Chem. Soc.* **1988**, *110*, 119. (b) Caridade Costa, J. M.; Bethell, D. *Port. Electrochim. Acta* **1993**, *11*, 73. (c) Caridade Costa, J. M.; Jeyashri B.; Bethell, D. *J. Electroanal. Chem.* **1993**, *351*, 259. (d) Allen, J. R.; Cynkowski, T.; Desai, J.; Bachas, L. G. *Electroanalysis* **1992**, *4*, 533.

(5) (a) Snyder, R.; Testa, A. C. *J. Lumin.* **1990**, *47*, 35. (b) Hirantani, K.; Nomoto, M.; Sugihara, H.; Okada, T. *Chem. Lett.* **1990**, 43. (c) Hirantani, K.; Nomoto, M.; Ohuchi, S.; Taguchi, K. *Bull. Chem.* Soc. *Jpn.* **1990**, *63*, 1349. (d) Wolfbeis, O. S.; Offenbacher, H. *Monatsh. Chem.* **1984**, *115*, 647. (e) Ogawa, S.; Tsuchiya, S. *Chem. Lett.* **1996**, 709.

(6) (a) Wassam, W. A.; Lim, E. C. *J. Mol. Struct.* **1978**, *47*, 129. (b) Brederek, K.; Forster, T.; Oesterlin, H. G. *Luminescence of Organic and Inorganic Materials*; Kallman, H. P., Sprunch, G. M., Eds.; Wiley: New York, 1962; p 161.

(7) (a) Montalti, M.; Prodi, L.; Zaccheroni, N. *J. Fluor.* **2000**, *10*, 71. (b) Prodi, L.; Bolletta, F.; Zaccheroni, N.; Watt, I. F.; Mooney, N. J. *Chem. Eur. J.* **1998**, 1090. (b) Leray, I.; Lefevre, J.-P.; Delouis, J. F.; Delaire, J.; Valeur, B. *Chem. Eur. J.* **2001**, *7*, 4590. (c) Zhang, H.; Han, L.-F.; Zachariasse, K. A.; Jiang, Y.-B. *Org. Lett.* **2005**, *7*, 4217. (d) Zhou, Z.; Farrni, C. J. *J. Am. Chem.* Soc. **2004**, *126*, 8862.

(8) (a) Larson, L. J.; Zinc, J. *Inorg. Chim. Acta* **1990**, *169*, 71 and references within. (b) Poiger, H.; Schlatter, C. *Analyst* **1976**, *101*, 808.

(9) (a) Yang, S. H.; Shon, O. J. Park, K. M.; Lee, S. S.; Park, H. J.; Kim, M. J.; Lee, J. H.; Kim, J. S. *Bull. Korean Chem. Soc.* **2002**, *23*, 1585. (b) Costero, A. M.; Andreu, R.; Monrabal, E.; Martinez-Manez, R.; Sancenon, F.; Soto, J. *J. Chem. Soc., Dalton Trans.* **2002**, 1769. (c) Chen, C. T.; Huang, W. P. *J. Am. Chem. Soc.* **2002**, *124*, 6246. (d) Xia, W. S.; Schmehl, R. H.; Li, C. J.; Mague, J. T.; Luo, C. P.; Guldi, D. M. *J. Phys. Chem. B* **2002**, *106*, 833. (e) Rurack, K.; Resch-Genger, U.; Bricks, J. L.; Spieles, M. *Chem. Commun.* **2000**, 2103. (f) J. Bourson, Badaoui, F.; Valeur, B. *J. Fluor.* **1994**, *4*, 275. (g) Bourson, J.; Pouget, J.; Valeur, B. *J. Phys. Chem.* **1993**, *97*, 4552. (h) Valeur, B.; Pouget, J.; Bourson, J. Kaschke, M.; Ernsting, N. P. *J. Phys. Chem.* **1992**, *96*, 6545.

[Ca·1](ClO$_4$)$_2$ (4). 1 (0.2 g, 0.5 mmol) was dissolved in 20 mL of acetonitrile. Calcium perchlorate tetrahydrate (0.156 g, 0.5 mmol) was dissolved in 10 mL of acetronitrile and added dropwise. The mixture was stirred for 2 h. All the solvents were evaporated under reduced pressure. The residue was redissolved in 20 mL of an acetonitrile−methanol (8:2) mixture and layered with diethyl ether. Yellow colored crystals were obtained. Yield: 65% (0.21 g). mp = 300 °C. ESI MS: Calcd for [Ca·**1**·ClO$_4$]$^+$ 537.95; found: 538.03 (M$^+$, 100%). ^{1}H NMR (CD$_3$CN, 25 °C): δ 3.89 (*s*, 8 H, CH$_2$−O); 4.12 (*t*, 4 H, CH$_2$−O, J = 4.5); 4.37 (*t*, 4 H, CH$_2$−O, J = 4.5); 7.48 (*m*, 2 H, Ar−H); 7.71 (*m*, 4 H, Ar−H). ^{13}C NMR (CD$_3$CN, 25 °C): δ 68.3, 70.4, 70.5, 70.6, 120.9, 121.7, 123.0, 135.5, 137.6, 159.8, 183.6, 188.8. Anal. Calcd for C$_{22}$H$_{22}$O$_{15}$CaCl$_2$: C, 41.45; H, 3.45%. Found: C, 42.10; H, 4.22%.

[Mn·1·CH$_3$CN·H$_2$O](ClO$_4$)$_2$ (5). 1 (0.25 g, 0.63 mmol) was dissolved in 20 mL of acetonitrile. Manganese(II) perchlorate hexahydrate (0.23 g, 0.63 mmol) was made in 10 mL of acetonitrile and added dropwise to the above solution. The color changed from yellow to orange, and after the solution was stirred for 1 h, all the solvent was removed by reduced pressure. The residue was dissolved in 5 mL of acetonitrile and layered with diethyl ether (40 mL). An orange-yellow colored precipitate was obtained. The entire product was dissolved again in 25 mL of acetonitrile, and diethyl ether was diffused into it. Fine orange crystals were obtained. Yield ≈ 0.33 g, 70%. ESI MS: Calcd for [Mn·**1**·ClO$_4$]$^+$ 552.80; found 552.28 (M$^+$, 100%). NMR signals are broad due to the paramagnetic manganese(II) center. Anal. Calcd for an air-dried sample of [Mn·**1**·CH$_3$CN·H$_2$O](ClO$_4$)$_2$ (C$_{24}$H$_{27}$Cl$_2$NO$_{16}$Mn): C, 40.52; H, 3.83; N, 1.97%. Found: C, 40.59; H, 3.60; N, 1.72%. After the sample was dryed at 100 °C under vacuum, elemental analyses was calculated for [Mn·**1**](ClO$_4$)$_2$ (C$_{22}$H$_{22}$Cl$_2$O$_{15}$Mn): C, 40.51; H, 3.37%. Found: C, 40.22; H, 3.58%.

[Zn·1·CH$_3$CN·H$_2$O](ClO$_4$)$_2$ (6). The synthesis of **6** is identical to the synthesis of **5**. Fine, orange-colored crystals were collected. Yield = 0.34 g (∼70%). ESI MS: Calcd for [Zn·**1**·ClO$_4$]$^+$ 563.26; found 562.97 (M$^+$, 100%). ^{1}H NMR (CD$_3$CN, 25 °C): δ 3.66−3.85 (*m* (broad), 12 H, CH$_2$−O); 4.00 (s, coordinated water and acetonitrile) 4.16 (*m*, 4 H, CH$_2$−O); 7.27 (*m*, 2H, Ar−H); 7.59 (*m*, 4 H, Ar−H). ^{13}C NMR (CD$_3$CN, 25 °C): δ 69.4, 69.6, 70.5, 70.7, 118.4, 119.2, 120.5, 124.2, 135.4, 135.9; 159.0, 183.9, 184.88. Anal. Calcd for an air-dried sample of [Zn·**1**·CH$_3$CN·H$_2$O](ClO$_4$)$_2$ (C$_{24}$H$_{27}$Cl$_2$NO$_{16}$Zn): C, 39.94; H, 3.77; N, 1.94%. Found: C, 39.74; H, 4.00; N, 1.68%. After the sample was dryed at 100 °C under vacuum, elemental analyses was calculated for [Zn·**1**·H$_2$O](ClO$_4$)$_2$ (C$_{22}$H$_{24}$Cl$_2$O$_{16}$Zn): C, 38.81; H, 3.52%. Found: C, 38.59; H, 4.15%.

Crystallography. Crystals of compound **2**, grown by vapor diffusion of MeOH/CH$_2$Cl$_2$, were mounted on a Siemens SMART Platform CCD diffractometer for data collection at 173(2) K using Mo K$_\alpha$ radiation. Final cell constants were calculated from the *xyz* centroids of typically more than 3000 reflections from the data collection after integration.[10] Structures were solved by direct methods using SIR92[11] or SHELXS-97[12] and refined using SHELXL-97.[13] One perchlorate was modeled as disordered over two positions (89:11). Crystallographic data for compounds **5** and **6**, grown by vapor diffusion of acetonitrile/ether, were collected at 203 and 295 K, respectively, using Mo K$_\alpha$ radiation on a Nonius CAD4 diffractometer. Refinement was completed using the WinGX suite of crystallographic software.[13,14] For **5** and **6**, which are isostructural, one perchlorate for both structures was modeled as disordered over two positions (83:17 for **5** and 61:39 for **6**). Carbons atoms 15 and 16 in the polyether chain were also found disordered and modeled in two positions (75:25 for **5** and 74:26 for **6**). Aromatic, methylene, and acetonitrile hydrogens were placed in calculated positions. Typically, one water hydrogen atom could be found in the difference map; however, the other hydrogen was placed in a calculated position and both constrained using SADI. Table 1 lists additional crystal and refinement information. Cambridge Crystallographic Data Centre deposition numbers are listed in Table 1. These data can be obtained free of charge via www.ccdc.cam.ac.uk/conts/retrieving.html (or from the CCDC, 12 Union Road, Cambridge CB2 1EZ, UK; fax: +44 1223 336033; e-mail: deposit@ccdc.cam.ac.uk).

Table 1. Crystallographic and Refinement Data for [**1**·Pb](ClO$_4$)$_2$ (**2**), [**1**·Mn(H$_2$O)(NCCH$_3$)](ClO$_4$)$_2$ (**5**), and [**1**·Zn(H$_2$O)(NCCH$_3$)](ClO$_4$)$_2$ (**6**)

	2	**5**	**6**
empirical formula	C$_{22}$H$_{22}$Cl$_2$PbO$_{15}$	C$_{24}$H$_{27}$Cl$_2$MnNO$_{16}$	C$_{24}$H$_{27}$Cl$_2$NO$_{16}$Zn
fw	804.49	711.32	721.74
temp	173(2) K	203(2) K	295(2) K
diffractometer	Seimens CCD	Nonius CAD4	Nonius CAD4
cryst syst	monoclinic	monoclinic	monoclinic
space group	*P*21/*n*	*P*21/*c*	*P*21/*c*
a, Å	8.0303(6)	10.132(2)	10.177(10)
b, Å	25.976(2)	11.8030(4)	11.977(6)
c, Å	12.1616(9)	23.999(7)	24.166(4)
β,°	94.9560(10)	95.75(2)	95.83(4)
V, Å^3	2527.4(3)	2855.5(10)	2930(1)
Z	4	4	4
density (calcd) g·cm^{-3}	2.114	1.655	1.636
absorb. coeff. mm^{-1}	6.965	0.730	1.099
F(000)	1560	1460	1480
θ range	1.57−27.49	1.7−25.0	1.3−25.0
index ranges	$-10 \le h \le 10$	$0 \le h \le 12$	$0 \le h \le 12$
	$-33 \le k \le 33$	$0 \le k \le 14$	$0 \le k \le 14$
	$-15 \le l \le 15$	$-28 \le l \le 28$	$-28 \le l \le 28$
independent reflns	5796	4991	5099
	[*R*(int) = 0.0378]	[*R*(int) = 0.0486]	[*R*(int) = 0.0284]
observed reflns	4980	3000	3061
max/min trans.	0.350 and 0.138	0.863 and 0.838	1.04 and 0.986
data/restr./param	5796/10/377	4991/19/435	5099/17/402
GOF	1.045	1.00	1.03
Final *R* indices [$I > 2\sigma(I)$]	R1 = 0.0266	R1 = 0.0488	R1 = 0.0673
	wR2 = 0.0500	wR2 = 0.0938	wR2 = 0.1729
R indices (all data)	R1 = 0.0365	R1 = 0.1254	R1 = 0.1288
	wR2 = 0.0525	wR2 = 0.1174	wR2 = 0.2084
peak and hole e.Å^{-3}	0.62 and −0.81	0.46 and −0.37	0.50 and −0.58
CCDC deposition no.	268922	268920	268921

Spectroscopy. Absorption spectra were recorded using a HP 8425A diode array spectrophotometer. Corrected (s/r) emission spectra were recorded using a SPEX Fluoromax fluorimeter. Fluorescence lifetimes were determined using a PTI TimeMaster instrument after excitation at 425 nm. Decay curves were fit to a single exponential and have an error of ±20%. Binding constants were determined according to eq 1.

$$Pb^{2+} + \mathbf{1} \leftrightarrow [Pb\cdot\mathbf{1}]^{2+} \quad (1)$$

UV/vis and emission spectra were run on a solution of **1** in acetonitrile (3 mL, 1×10^{-4} M) and microliter aliquots of M^{2+} salt solution were added. Fitting was completed using an Excel spreadsheet, where values of the binding constants were obtained by simulation of the data using the equilibrium constant and I_∞ as

(10) *SAINT V6.1*; Bruker Analytical X-ray Systems: Madison, WI, 1999.
(11) Altomare, A.; Cascarno, G.; Giacovazzo, C.; Gualardi, A. *J. Appl. Cryst*. **1993**, *26*, 343.
(12) *SHELXTL-Plus V5.10*; Bruker Analytical X-ray Systems: Madison, WI, 1998.
(13) Sheldrick, G. M. *SHELX97 − Programs for Crystal Structure Analysis (Release 97-2)*; Institüt für Anorganische Chemie der Universität: Göttingen, Germany, 1998.
(14) *WinGX: An Integrated System of Windows Programs for the Solution, Refinement, and Analysis of Single-Crystal X-ray Diffraction Data*, Ver. 1.63. Farrugia, L. J. *J. Appl. Cryst*. **1999**, *32*, 837.

Scheme 1

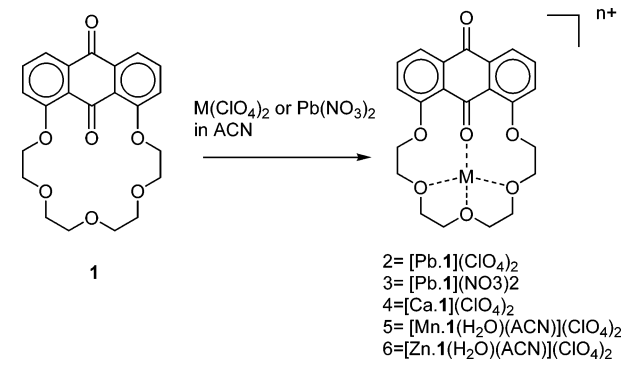

adjustable parameters. Error in I_∞ is small since binding constants are large and have a level maximum plateau.

Results

A. Synthesis and Changes to Absorbance Spectra. Addition of 1 equiv of a metal perchlorate or nitrate salt to **1** in acetonitrile yields the 1:1 metal/ligand complexes **2**−**6** (Scheme 1), which have been characterized by electrospray mass spectrometry, elemental analyses, NMR, and X-ray crystallography. The number of solvent molecules coordinated to the encapsulated metal ions in these complexes is dependent on the degree of dryness. [Pb·**1**]$(ClO_4)_2$ (**2**) and [Ca·**1**]$(ClO_4)_2$ (**4**), both recrystallized from acetonitrile, and [Pb·**1**]$(NO_3)_2$ (**3**), recrystallized from DMF/ether, do not show any degree of solvation as the elemental analyses are almost identical before and after drying at 100 °C in a vacuum. The nitrate salt is also significantly less soluble in acetonitrile than the perchlorate salt. The elemental analyses results of the Mn^{2+} and Zn^{2+} complexes crystallized from acetonitrile indicate the addition of one water and one acetonitrile molecule to these complexes, [M·**1**(H_2O)(ACN)]-$(ClO_4)_2$, which has been confirmed by crystallography (*vida infra*). Elemental analyses results of **5** and **6** after drying at 100 °C in a vacuum indicate the Mn complex loses both the water and the acetonitrile to become [Mn·**1**]$(ClO_4)_2$, while the zinc complexes loses only the acetonitrile, leaving [Zn·**1**(H_2O)]$(ClO_4)_2$. The degree of solvation has a profound influence on the luminescence efficiency of these complexes in the solid state.

Figure 1 shows the absorbance changes that occur upon titration of **1** with $Pb(ClO_4)_2$ in acetonitrile. A clean isosbestic point is observed with the addition of 1 equiv of Pb^{2+}, reinforcing the 1:1 metal/ligand stoichiometry of this complex in solution. The λ_{max} does not continue to shift after the addition of 1 equiv of lead. The red-shift in λ_{max} is attributed to the stabilization of the excited state by a bound cation in immediate juxtaposition to the intraannular carbonyl oxygen.[15]

B. Crystallography. We were able to prepare crystals of **1** combined with Pb, Mn, and Zn perchlorate salts that were suitable for single-crystal X-ray crystallography. The crystallographic results confirmed that 1:1 metal/ligand stoichiometries were produced in all cases. Crystallization of [Pb·**1**]$(ClO_4)_2$ proved difficult, and recrystallization from acetonitrile produced only fibrous microcrystals, too small for diffraction. Figure 2A shows the crystal structure of [Pb·**1**]$(ClO_4)_2$ grown from methanol/CH_2Cl_2. The Pb^{2+} cation is located in the center of the macrocycle, coordinated to four ligand oxygens, including the intraannular carbonyl oxygen. Two perchlorate anions, one on each side of the macrocycle (Figure 2B), are bound to the Pb^{2+} ion as well. One perchlorate is bound to the lead ion through one oxygen atom (Pb1−O12 = 2.707 Å), while the second perchlorate chelates the lead ion via two oxygen atoms (Pb1−O8 = 2.639 Å and Pb1−O9 = 2.754 Å). The total coordination number for the lead equals seven. The carbonyl oxygen coordinated

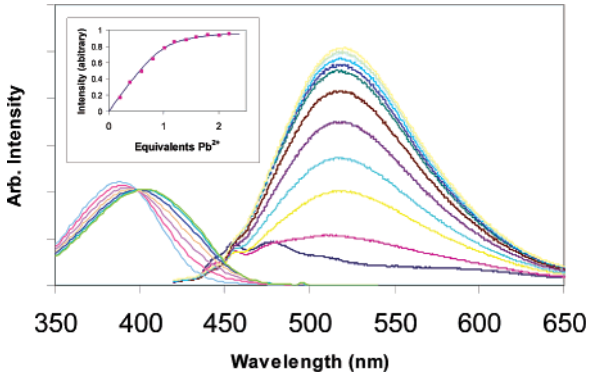

Figure 1. UV/vis and fluorescence titration of **1** with $Pb(ClO_4)_2$. Each addition is 0.2 equiv of $Pb(ClO_4)_2$ in acetonitrile. Excitation at 398 nm (ϵ_{398} = 6800 M^{-1} cm^{-1}). Inset is a plot of emission intensity vs equivalents of Pb^{2+} added.

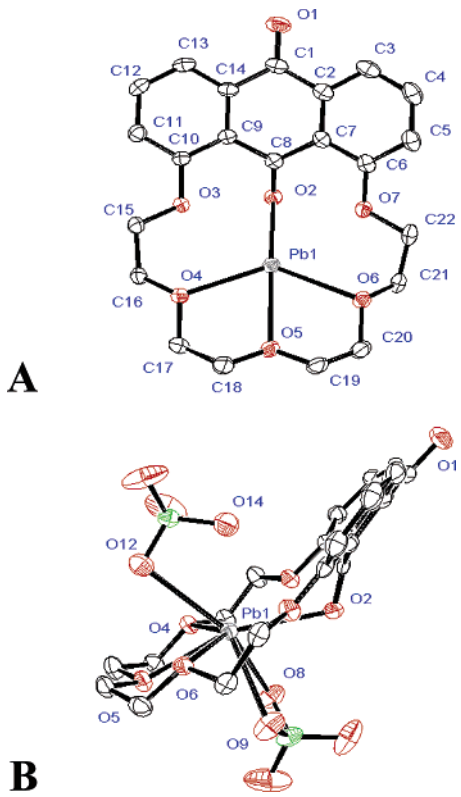

Figure 2. (A) Thermal ellipsoid (50%) diagram of [**1**·Pb]$(ClO_4)_2$. Perchlorate anions and hydrogen atoms have been excluded for clarity. (B) Side view showing both coordinated perchlorate anions.

(15) Wehry, E. L. *Practical Fluorescence*; Guilbault, G. G., Ed.; Marcel Dekker: 1990; p 127.

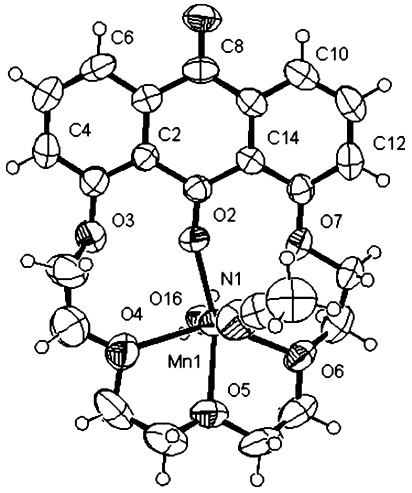

Figure 3. Thermal ellipsoid (50%) diagram of $[\mathbf{1}\cdot Mn\cdot H_2O\cdot CH_3CN]^{2+}$ cation. The perchlorate counteranions have been removed for clarity.

Table 2. Selected Bond Distances(Å)

	2 (Pb)		**5** (Mn)	**6** (Zn)
temp (K)	173		203	295
M−O2 (...O═C)	2.577(2)		2.104(4)	2.078(4)
M−O4 (...O−CH_2)	2.617(2)		2.344(6)	2.310(8)
M−O5 (...O−CH_2)	2.506(2)		2.212(3)	2.153(4)
M−O6 (...O−CH_2)	2.609(2)		2.270(4)	2.218(5)
M−O3 (...O-aryl)	3.036		3.722	3.797
M−O7 (...O-aryl)	3.011		2.833	2.791
M−O8 (...ClO_4)	2.639(3)	M−OH_2	2.107(4)	2.016(5)
M−O9 (...ClO_4)	2.754(3)	M−$NCCH_3$	2.158(5)	2.018(7)
M−O12 (...ClO_4)	2.701(6)	C≡N	1.122(6)	1.114(8)
O2−C8 (O═C)	1.232(4)		1.230(5)	1.222(6)
O1−C1 (O═C)	1.223(4)		1.222(5)	1.228(7)

to the lead cation (Pb1−O2 = 2.577 Å) is significantly bent out of the anthraquinone plane (Figure 2B), almost certainly to increase the coordination space within the macrocycle. Figure 2B also shows that the anthraquinone system is not planar. Least-squares planes defined by the two aromatic rings in the anthraquinone are offset by a dihedral angle of 20.0(2)° to one another. Other important bond distances are listed in Table 2. We have not been able to grow crystals of the $[Pb\cdot\mathbf{1}](NO_3)_2$ complex so far using either evaporative or diffusion techniques due to the limited solubility of this complex or by slow diffusion of dilute $TEANO_3$ into $[Pb\cdot\mathbf{1}](ClO_4)_2$, which has produced only clusters of fibrous microcrystals.

Vapor diffusion of ethyl ether into acetonitrile solutions of **5** or **6** produces crystals that are isostructural. The structure of these Mn^{2+}- and Zn^{2+}-containing complexes is dramatically different from the lead complex above, as both the coordination geometry of the metal centers and the overall structure of the macrocycle have changed. Figure 3 shows the structure of the Mn^{2+} complex. Four macrocyclic oxygens again coordinate to the manganese; however, the coordinating perchlorate anions have been substituted by a water molecule and an acetonitrile molecule, above and below the plane of the macrocycle. The Mn^{2+} and Zn^{2+} metal centers are not centered within the macrocyclic cavity in these structures, where, as in the case of Mn^{2+}, the cation is displaced toward O7 (Mn−O7 = 2.83 Å, as opposed to Mn−O3 = 3.72 Å). Although the M−O7 bond is on average 0.6 Å longer than the other M−O bonds within the coordination sphere, the coordination geometry can be described as a combination of six-coordinate distorted octahedral and seven-coordinate *pseudo*-pentagonal bipyramidal.

Table 3. Photophysical Characteristics of $[M\cdot\mathbf{1}]^{2+}$ Perchlorate Complexes in Acetonitrile and in the Solid State at 21 °C

M	1	Ca^{2+}	Mn^{2+}	Pb^{2+}	Pb^{2+} nitrate	Zn^{2+}
λ_{vis} (acetonitrile, nm)	385	408	390	404	404	390
log K_b	–	5.8 ± 0.3	–	5.5 ± 0.3	–	–
λ_{em} (acetonitrile, nm)	480	500	–	515	–	–
λ_{em} (solid state, nm)	–	509 (strong)	537 (weak)	493 (strong)	493 (weak)	544 (strong)
Stokes shift (cm^{-1})		4900	7000	4500	4500	7300
size		0.99	0.91	1.32		0.83
τ (ns, deaerated)		<0.5		<0.5		
quantum yield		0.016		0.022		

What is most striking about this complex, however, is that the anthraquinone is virtually planar. In fact, this appears to be the reason the metal is not centered within the cavity, as the intraannular carbonyl oxygen that extends into the polyether ring constrains the M^{2+} ion to be offset. The dihedral angle formed between the two aromatic ring planes of the anthraquinone averages only 1.6(2)° in these two structures. With a planar anthraquinone system, π-stacking is also observed within dimers throughout the crystal with a ~3.6 Å separation of the staggered, π-stacked anthraquinone units. Hydrogen-bonding interactions are formed between the water and a neighboring carbonyl oxygen (O16−O1 = 2.74 Å) and also to a neighboring perchlorate (O16−O15 = 2.72 Å).

C. Fluorescence Studies and Cation Affinity. Concomitant with the shift in the absorbance maximum of **1** upon addition of $Pb(ClO_4)_2$ in acetonitrile, a dramatic increase in fluorescence at 515 nm occurs as well (Figure 1). The emission intensity crests with the addition of 1 equiv of Pb^{2+} (inset, Figure 1), confirming the stoichiometry of 1:1 complex formation, as the absorbance and crystallographic results also confirm. Addition of calcium perchlorate to **1** in acetonitrile also produces a large emission enhancement and a similar red-shift in absorbance. Addition of manganese or zinc perchlorate to **1** does not produce large emission enhancements, and only a decrease in the absorbance maximum with no shift in wavelength is observed. From both the absorption and emission data, average binding constants for calcium and lead complexation were determined and are provided in Table 3.

Addition of good coordinating anions to solutions of $[Pb\cdot\mathbf{1}](ClO_4)_2$ in acetonitrile also quench the emission of this adduct. Figure 4 shows the addition of $TEANO_3$ to $[Pb\cdot\mathbf{1}](ClO_4)_2$, where emission is almost completely quenched after the addition of 2 equiv of nitrate. The Stern−Volmer plot (inset, Figure 4) also yields a straight line through the addition of 1 equiv of nitrate.

Figure 5 compares the selectivity of **1** with different perchlorate salts. In anhydrous acetonitrile, 2 equiv of a dried perchlorate salt were added to **1** and the emission spectrum recorded. Emission change is most sensitive for the addition

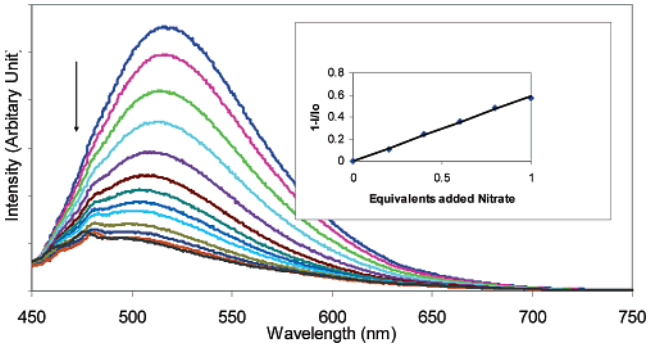

Figure 4. Fluorescence Titration of 1.0×10^{-4} M [**1**·Pb]$(ClO_4)_2$ in acetonitrile with 0.2 equiv additions of tetraethylammonium nitrate ($TEANO_3$). Inset is the Stern−Volmer plot for addition of the first equivalent of added nitrate, slope = 6100 M^{-1}.

of lead ion, and selectivity is high for lead, with potential interference occurring mainly from alkaline earth metals, chiefly calcium ion. When the hydrated perchlorate salts were used instead, no large difference in fluorescence intensity was observed.

D. Solid-State Fluorescence Studies. To remove the effects of solvation on luminescence, all samples were dried at 100 °C under vacuum and the solid-state emission spectra were recorded. Because uneven surface coverage and slight changes in the angle of incidence of the excitation beam can cause difficulty in quantifying exact luminescence intensity, only λ_{em} and relative emission intensities are reported for solid samples in Table 3 and Figure 6. Also, the best fit of the elemental analyses results suggest that [Zn·**1**]$(ClO_4)_2$ retains one water of hydration even after drying at 100 °C; however, a negligible nitrogen percentage indicates that the acetonitrile has been removed. Microanalysis results of the dried Ca(II), Mn(II), and Pb(II) complexes show that no solvent remains.

Discussion

The critical feature responsible for initiating luminescence in **1** is the degree of electropositive charge experienced by the intraannular carbonyl oxygen, which in turn controls the inversion of nπ^* and $\pi\pi^*$ excited states in the lumophore. Conditions that influence the degree of positive charge include the charge of the guest cation, the degree of solvation within the coordination sphere of the bound cation, and the coordinating ability of the counteranion. From Figure 5, compound **1** shows very limited luminescence enhancement in the presence of lithium or sodium ion, while much larger enhancements are observed for the dipositive cations Ca(II) and Pb(II). The luminescence turn-on threshold in this system appears to be limited to cations with oxidation states of +2 charge or greater. Doubly charged cations do not always produce large luminescence enhancements, however. The transition metal ions Cu(II), Ni(II), and Mn(II) show minimal, or negative enhancements in fact, which we attribute to the presence of low-lying d−d transitions that effectively quench emission internally. This phenomenon has previously been observed.[8a]

Surprisingly, Zn(II) ion, containing a full complement of d electrons, also shows limited luminescence enhancement. Here the elemental analyses and the crystallographic results show considerable differences between the coordination environments of the weakly luminescent Mn(II) and Zn(II) complexes and the luminescent Ca(II) and Pb(II) complexes. The Mn(II) and Zn(II) complexes of **1** contain two additional solvent molecules in the coordination sphere that are not present in the cases of Pb(II) and Ca(II). The electron-donating ability of these additional ligands we feel reduces the electropositive character of the complexed metal ion and prevents inversion of nπ^* and $\pi\pi^*$ excited states.

This same effect is observed when better coordinating anions such as nitrate or chloride are added to solutions of [Pb·**1**]$(ClO_4)_2$. Emission from [Pb·**1**]$(ClO_4)_2$ solution is completely quenched after 1−2 equiv of nitrate is added (Figure 4), and no precipitate is formed. With the addition of nitrate, we have calculated both the Stern−Volmer constant (K_{SV} = ~6000 M^{-1}) and the lifetime of [Pb·**1**]-$(ClO_4)_2$ in deaerated solvent (τ_o = <0.5 ns) and conclude that the calculated bimolecular quenching constant ($k_q = K_s/$

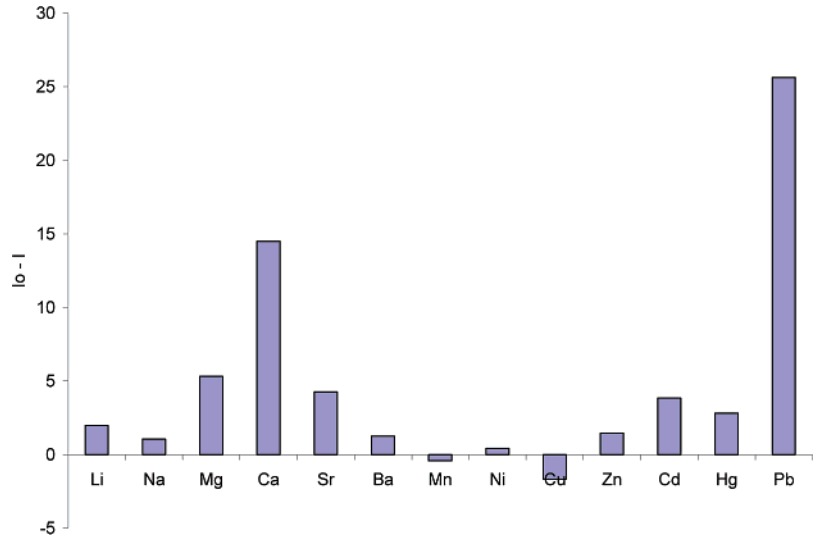

Figure 5. Fluorescence changes of **1** after addition of 2 equiv of metal perchlorate salts. Excitation wavelength was 398 nm and the emission intensity changes were calculated at 515 nm. **1** = 1.0×10^{-4} M; M^{2+} = 2.0×10^{-4} M.

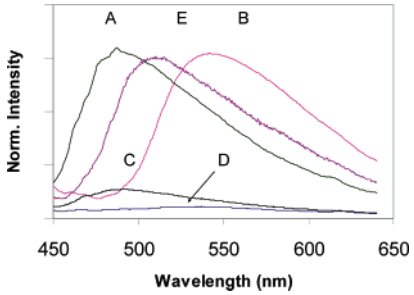

Figure 6. Solid-state emission spectra of (A) [**1**·Pb]$(ClO_4)_2$, (B) [**1**·Zn]$(ClO_4)_2$·H_2O, (C) [**1**·Pb]$(NO_3)_2$, (D) [**1**·Mn]$(ClO_4)_2$, and (E) [**1**·Ca]$(ClO_4)_2$. Excitation was at 420 nm. Emission intensities due to different surface coverage and angle of incidence changes are relatively arbitrary.

τ_o, $\sim 1 \times 10^{13}$ M^{-1} s^{-1}) is approximately 1000 times faster than what is diffusion allowed.[16] Hence, this eliminates dynamic quenching and supports the formation of a ground-state, dark complex with the better coordinating anion. Again, strong coordination of negatively charged anions to the metal center reduces the electropositive character and prevents luminescence. Pb(II) and Ca(II) perchlorate salts of **1** show the greatest luminescence enhancements because they have high charge, large affinities, and presumably only weakly associate with solvent and perchlorate counterions in solution.

The effect of increasing the amount of electropositive charge on the cation can also be observed in the solid-state luminescence spectra. Most notably, the Zn(II) complex changes from being virtually nonluminescent in acetonitrile solution to being strongly luminescent in the solid state. The loss of the coordinating acetonitrile ligand in the case of zinc apparently increases the charge experienced by the lumophore and allows inversion of exited states to occur. Even though the dried Mn(II) complex has lost both water and acetonitrile ligands, luminescence remains poor since deactivation by accessible d−d transitions is still expected. Ca(II) and Pb(II) complexes remain strong emitters in the solid-state.

The sense that nπ^* and $\pi\pi^*$ states are completely inverted in this system is probably not the case. The quantum yields are relatively low ($\sim$2%, Table 3), indicating that the energy difference between the nπ^* and $\pi\pi^*$ states has been reduced, but a significantly larger quantum yield is necessary to predict complete inversion. The quantum yields observed here are similar to that found for [**1**·H_3O^+](ClO_4) (Φ = 1.4%),[3b] also indicating that the quantum yield remains a function of the host more than the identity of the electropositive guest cation.

A second important feature to point out is that different cations produce different Stokes shifts when complexed by **1**. This feature allows for possible identification of metal ions in solution and even identification of mixtures of ions via ratiometric analysis. Changes in Stokes shifts follow conventional theory that polar excited states are sufficiently long-lived and undergo environmental relaxation, stabilizing the excited state and result in significant red-shifts in emission. This is commonly observed when solvent polarity is increased: more-polar solvents exhibiting the largest Stokes shifts. In this system, however, the solvent (acetonitrile) remains unchanged and it is the bound cation that changes. Table 3 shows that the largest Stokes shifts occur for the smallest dipositive cations. Smaller cations have the greatest charge densities (charge/size ratios) and have the greatest potential of stabilizing the adjacent excited state of the lumophore, causing large Stokes shifts. Large cations such as Pb(II) which form long bonds within the macrocycle stabilize the excited state the least, causing less of a red-shift. This pattern is mirrored in the solid-state emission results as well; however, all the solid-state maxima are blue-shifted as compared to the solution emission maxima since any stabilizing influence by the polar acetonitrile solvent has been subtracted. From our previous work, encapsulation of hydronium ion by **1** forms strong hydrogen bonds with the intraannular carbonyl oxygen, resulting in a large luminescence enhancement at 570 nm.[3d] The donation of a hydrogen-bonded proton from the hydronium ion represents an interaction with one of the largest charge densities possible and continues the trend by producing an even larger Stokes shift for **1**. When acetonitrile/aqueous $HClO_4$ is replaced by concentrated sulfuric acid, direct protonation of the carbonyl oxygen is observed ($pK_a \approx -5.0$) and a new luminescence band grows in at 650 nm, which may represent the limit of the red-shift in this system.[3b] Planarity of the anthraquinone lumophore does not appear to be involved with luminescence turn-on thresholds, namely because the Zn complex which is virtually planar ($\sim$2°) is not luminescent and the Ca(II) and Pb(II) complexes which are significantly bent ($\sim$20°) are the most luminescent. For [**1**·H_3O^+](ClO_4), the hydronium adduct exhibits an even larger bend in the anthraquinone plane ($\sim$23.2°) and produces a 40-fold increase in emission intensity.[3d] The encapsulation of large cations by the polyether chain and the immobilization of the intraannular carbonyl oxygen lends support to the argument that increased structural rigidity within the complex leads to large increases in luminescence as well.

Conclusions

Inversion of excited states is a luminescence switching mechanism capable of detecting transition and heavy metal ions in solution and the solid state. Complexation of metal ions within this host system is robust and leads to large shifts in emission maxima depending on the identity of the ion. Judicious choice of the counteranion is also important in order for luminescence to occur; however, the quenching of luminescence by anions is considered to be a detection method in itself (an anion sensor). The macrocycle we have studied is most sensitive to cations with high charge, cations that form long bonds within the host, and cations which do not coordinate solvent, which is necessary for the inversion of excited states. Because the lumophore and the receptor are integrated together within these sensors, it should be relatively easy to tailor the size/shape of the receptor to increase selectivity for different cations and to influence the corresponding Stokes shifts. Both larger and smaller polyether rings attached to the 1 and 8 positions of anthraquinone

(16) Lakowicz, J. R. *Principles of Fluorescence Spectroscopy*, 2nd ed.; Kluwer Academic Press: New York, 1999; p 255.

have already been reported.[4c−d,17] We are currently studying these other cyclic analogues and open-ring (bipodand) anthraquinone systems to understand more about the structure−property relationships of this new type of luminescence sensor.

Acknowledgment. The authors thank the National Science Foundation (0082978) and the South Dakota 2010 Initiative for financial support. We also thank the University of South Dakota and NSF-EPSCOR (9720642 and 0091948) for the purchase and upgrade of a Nonius CAD4 X-ray diffractometer and Benjamin Kucera and the University of Minnesota X-ray Diffraction Laboratory for the structure determination of [Pb·**1**]$(ClO_4)_2$. The authors also thank the reviewers for helpful comments.

Supporting Information Available: Crystallographic data in cif format. This material is available free of charge via the Internet at http://pubs.acs.org.

IC051672Z

(17) (a) Kumar, S.; Hundal, G. Bhalla, V.; Hundal, M. S.; Singh, H. *J. Chem. Res.* **1998**, 794. (b) Kim, H.; Schall, O. F.; Fang, J.; Trafton, J. E.; Lu, T.; Atwood, J. L.; Gokel, G. W. *J. Phys. Org. Chem.* **1992**, *5*, 482.